Applied Physics Letters

RESEARCH ARTICLE | JULY 31 2024

Time-resolved imaging of GHz acoustic vibrations at arbitrary frequencies using asynchronous periodic probe laser pulses

Osamu Matsuda ; Shohei Ueno; Motonobu Tomoda ; Paul H. Otsuka; Oliver B. Wright

Appl. Phys. Lett. 125, 052201 (2024)
https://doi.org/10.1063/5.0218494

AIP Publishing

Applied Physics Letters ARTICLE pubs.aip.org/aip/apl

Time-resolved imaging of GHz acoustic vibrations at arbitrary frequencies using asynchronous periodic probe laser pulses

Cite as: Appl. Phys. Lett. **125**, 052201 (2024); doi: 10.1063/5.0218494
Submitted: 11 May 2024 · Accepted: 17 July 2024 ·
Published Online: 31 July 2024

View Online Export Citation CrossMark

Osamu Matsuda,[1,a] Shohei Ueno,[1] Motonobu Tomoda,[1] Paul H. Otsuka,[1] and Oliver B. Wright[2,3]

AFFILIATIONS

[1]Division of Applied Physics, Graduate School of Engineering, Hokkaido University, Sapporo 060-8628, Japan
[2]Hokkaido University, Sapporo 060-0808, Japan
[3]Graduate School of Engineering, Osaka University, 2-1 Yamadaoka, Suita, Osaka 565-0871, Japan

[a]Author to whom correspondence should be addressed: omatsuda@eng.hokudai.ac.jp

ABSTRACT

We present a technique for imaging gigahertz surface acoustic waves in the time domain at arbitrary frequencies, in which acoustic waves are excited asynchronously to the optical probe pulse train used to detect them. We apply this approach to the two-dimensional imaging of electrically excited single-frequency surface acoustic waves on a GaAs substrate with a deposited interdigital transducer. This technique significantly increases the possible fields of application for gigahertz acoustic wave device imaging.

Surface acoustic waves in the megahertz-to-gigahertz frequency region are widely exploited in, for example, filters for cellphone communication systems,[1] sensor devices for gas molecules,[2] and data processing devices.[3] For such applications, it is important to visualize the propagation of the surface acoustic waves in the time domain.

Time- and spatially resolved imaging of acoustic fields is a mature subject.[4–16] In particular, for non-contact probing, ultrafast all-optical methods have been proposed[8,17–22] that exploit the optical pump–probe technique using a periodic ultrashort light pulse train from a mode-locked laser. Pump light pulses are focused on the sample surface to generate acoustic waves, and delayed probe light pulses detect the resulting surface displacement. By scanning the probe light spot position for a fixed pump light spot position and by scanning the delay time between the pump and probe light pulses, spatiotemporal imaging of the acoustic field with micrometer spatial and picosecond temporal resolution becomes possible. This technique relies on the synchronization of the generated acoustic waves and the probe light pulses: since both the pump and probe light pulses originate from the same pulsed laser and possess a fixed repetition rate (typically $\sim$80 MHz), their synchronization is assured. The additional use of lock-in detection and a pump-beam modulation technique greatly improves the signal-to-noise ratio. For the case of electrical excitation of acoustic waves by gigahertz transducers, it has been shown that ultrafast optical imaging of the acoustic field is possible by synchronizing the electric excitation with the probe light repetition rate.[23]

In practical applications, however, the acoustic waves are often generated by an electrical source independent of (and thus not synchronized with) the probe light pulses. One example would be the measurement of a surface acoustic wave filter driven by a radio frequency (RF) signal source. However, if one probes such acoustic waves with periodic laser pulses asynchronous to the acoustic vibration, it might appear at first sight that a null measurement on average would result, since each probe laser pulse detects a different phase of the acoustic oscillation.

In this paper, we propose a technique to avoid such a null measurement in a pump–probe setup by use of a time-domain heterodyne system involving a shift in frequency while maintaining sensitivity to the acoustic phase. Detection is achieved with an ultrafast two-dimensional optical interferometric imaging system for surface displacement. We demonstrate its feasibility by the spatiotemporal imaging of $\sim$1 GHz single-frequency surface acoustic waves on a GaAs substrate fitted with an interdigital transducer and driven by an asynchronous electric signal.

We first describe the principle of the asynchronous optical probing. This method is an extension of one previously developed for monitoring arbitrary-frequency acoustic fields using optical pumping and probing.[24,25] Consider the example of a sample containing an interdigital transducer for surface acoustic wave generation that is driven by an RF signal source at frequency f_0. The generated acoustic field is monitored optically using a periodic train of ultrashort light pulses of repetition frequency f_{rep}. The acoustic field strength, for example the surface displacement or the surface particle velocity, is converted by the measurement system to an electronic signal, which is fed to a dual-phase lock-in amplifier that outputs both in-phase and quadrature components. The reference signal of the lock-in amplifier is obtained from f_0 and f_{rep}, as described below.

We consider the case of a single-frequency acoustic field $u(x, y, t)$ at angular frequency $\omega_0 = 2\pi f_0$,

$$u(x, y, t) = A(x, y)\cos[-\omega_0 t + \phi(x, y)], \tag{1}$$

where t is the elapsed time (not to be confused with the delay time τ). The amplitude A and phase ϕ, both functions of position, are the quantities of interest. The field u is probed by periodic probe pulses at repetition angular frequency $\omega_{\mathrm{rep}} = 2\pi f_{\mathrm{rep}}$ and oscillation period $T = 1/f_{\mathrm{rep}}$. Probe light pulses are subject to delay τ (see the description of the experimental method below for details). The contribution to the probed acoustic field associated with the Nth probe pulse is given by

$$\begin{aligned} u_N(x, y, \tau) &= u(x, y, NT + \tau) \\ &= A(x, y)\cos[-\omega_0(NT + \tau) + \phi(x, y)], \end{aligned} \tag{2}$$

which we can consider as a signal component input to the lock-in amplifier. The reference signal for the lock-in amplifier is constituted as follows: we first mix the output of a fast photodiode, which detects the probe laser pulses and outputs frequency components at integer multiples of f_{rep}, with the output of the RF electrical signal source at the single frequency f_0. We use the lowest frequency component,

$$F = |f_0 - n_0 f_{\mathrm{rep}}|, \tag{3}$$

obtained by means of a mixer as the lock-in reference signal. The integer $n_0 > 0$ is chosen so that F is minimized: in general, $F < f_{\mathrm{rep}}/2$. We define the angular frequency $\Omega = 2\pi F$ for later use. Hereafter, we assume f_0 is not an exact integer multiple of f_{rep}. This is a limitation of the method: it is not possible to observe the vibration at such frequencies.

The in-phase (X) and quadrature (Y) outputs of the lock-in amplifier are proportional to

$$\begin{aligned} X(x, y, \tau) &= \overline{u_N(x, y, \tau)\cos[\Omega(NT + \tau)]} \\ &= A\,\overline{\cos[-\omega_0(NT + \tau) + \phi]\cos[\Omega(NT + \tau)]} \\ &= \frac{A}{2}\Big\{\overline{\cos[(\Omega - \omega_0)(NT + \tau) + \phi]} \\ &\quad \overline{+\cos[(\Omega + \omega_0)(NT + \tau) - \phi]}\Big\} \\ &= \frac{A}{2}\cos(-n_0\omega_{\mathrm{rep}}\tau + \phi), \end{aligned} \tag{4}$$

and

$$\begin{aligned} Y(x, y, \tau) &= \overline{u_N(x, y, \tau)\sin[\Omega(NT + \tau)]} \\ &= A\,\overline{\cos[-\omega_0(NT + \tau) + \phi]\sin[\Omega(NT + \tau)]} \\ &= \frac{A}{2}\Big\{\overline{\sin[(\Omega - \omega_0)(NT + \tau) + \phi]} \\ &\quad \overline{+\sin[(\Omega + \omega_0)(NT + \tau) - \phi]}\Big\} \\ &= \begin{cases} \dfrac{A}{2}\sin(-n_0\omega_{\mathrm{rep}}\tau + \phi) & (\omega_0 > n_0\omega_{\mathrm{rep}}) \\ -\dfrac{A}{2}\sin(-n_0\omega_{\mathrm{rep}}\tau + \phi) & (\omega_0 < n_0\omega_{\mathrm{rep}}) \end{cases} \\ &= \frac{A}{2}\mathrm{sgn}(\omega_0 - n_0\omega_{\mathrm{rep}})\sin(-n_0\omega_{\mathrm{rep}}\tau + \phi). \end{aligned} \tag{5}$$

The time averaging $\overline{s_N}$ is defined as

$$\overline{s_N} = \frac{1}{N_{\mathrm{max}}}\sum_{j=0}^{N_{\mathrm{max}}-1} s_j$$

for the series s_j $(j = 0, 1, 2, \ldots)$ with a sufficiently large integer N_{max} whose value increases with the lock-in time constant.

Equations (4) and (5) can be combined as follows:

$$\begin{aligned} Z(x, y, \tau) &= X(x, y, \tau) + iY(x, y, \tau) \\ &= \frac{A(x, y)}{2}\exp\{i\,\mathrm{sgn}(\omega_0 - n_0\omega_{\mathrm{rep}})(-n_0\omega_{\mathrm{rep}}\tau + \phi(x, y))\}. \end{aligned} \tag{6}$$

The complex signal $Z(x, y, \tau)$ exhibits oscillations at the angular frequency $n_0\omega_{\mathrm{rep}}$ with respect to τ when $\omega_0 > n_0\omega_{\mathrm{rep}}$ or at the angular frequency $-n_0\omega_{\mathrm{rep}}$ when $\omega_0 < n_0\omega_{\mathrm{rep}}$.

So far, we have considered the acoustic field component at angular frequency ω_0. However, the lock-in detection (of periodic probe light pulses) is also sensitive to vibrations at $n\omega_{\mathrm{rep}} + l\Omega$, where n is an arbitrary positive integer with $l = \pm 1$ or $n = 0$ with $l = 1$.[25] This sensitivity becomes evident on replacing ω_0 in Eq. (1) by $n\omega_{\mathrm{rep}} + l\Omega$ while maintaining the required lock-in reference frequency $F = 2\pi/\Omega$. Furthermore, in the last lines of Eqs. (4) and (5), $n_0\omega_{\mathrm{rep}}\tau$ and $\mathrm{sgn}(\omega_0 - n_0\omega_{\mathrm{rep}})$ are replaced with $n\omega_{\mathrm{rep}}\tau$ and l, respectively. The complex signal $Z(x, y, \tau)$ can then be written as

$$Z_{n,l}(x, y, \tau) = \frac{A_{n,l}(x, y)}{2}\exp\{il[-n\omega_{\mathrm{rep}}\tau + \phi_{n,l}(x, y)]\}, \tag{7}$$

where Z, A, and ϕ are in this case indexed with n, l. By use of the integer index n', the temporal Fourier transform given by

$$\begin{aligned} F_{n'} &= \frac{1}{T}\int_0^T Z_{n,l}\exp(in'\omega_{\mathrm{rep}}\tau)\mathrm{d}\tau \\ &= \begin{cases} \dfrac{A_{n,l}}{2}e^{i\phi_{n,l}}\delta_{n,n'} & (l = 1), \\ \dfrac{A_{n,l}}{2}e^{-i\phi_{n,l}}\delta_{n,-n'} & (l = -1), \end{cases} \end{aligned} \tag{8}$$

can be used to extract $A_{n,l}$ and $\phi_{n,l}$ from $Z_{n,l}$. The quantity $F_{n'}$ with $n' \geq 0$ is related to detected vibrations with $l = 1$ (at $\omega = n'\omega_{\mathrm{rep}} + \Omega$, termed the upper sideband, USB), whereas $F_{n'}$ with $n' < 0$ is related to detected vibrations with $l = -1$ (at $\omega = -n'\omega_{\mathrm{rep}} - \Omega$, termed the lower sideband, LSB). Detected vibrations at ω_0 are included for the case $l = \mathrm{sgn}(\omega_0 - n_0\omega_{\mathrm{rep}})$, in which case one can write $\omega_0 = n_0\omega_{\mathrm{rep}} + l\Omega$.

For the more general case of an acoustic field made up of a superposition of different n, l components, Eqs. (1) and (6) are generalized to

$$\begin{aligned} u(x, y, t) &= \sum_{n,l} A_{n,l}(x, y)\cos\{-(n\omega_{\mathrm{rep}} + l\Omega)t + \phi_{n,l}(x, y)\}, \\ Z(x, y, \tau) &= \sum_{n,l} Z_{n,l}(x, y, \tau). \end{aligned} \tag{9}$$

In this case, Eq. (8) can again be used, provided that one replaces $Z_{n,l}$ with Z. For excitation of the sample at a single angular frequency ω_0, in the linear regime one would expect a detected vibration only at

$\omega = \omega_0$. In practice, spurious frequency components at $\omega \neq \omega_0$ may appear because of experimental considerations, as discussed later in conjunction with Fig. 3(b).

Spatiotemporal Fourier analysis of $Z(x, y, \tau)$ can be achieved as follows:

$$F(k'_x, k'_y, n'\omega_{\mathrm{rep}}) = \frac{1}{(2\pi)^2 T} \int\int \mathrm{d}x\mathrm{d}y \int_0^T \mathrm{d}\tau \times Z(x, y, \tau) \exp\{-i(k'_x x + k'_y y - n'\omega_{\mathrm{rep}}\tau)\}. \tag{10}$$

The utility of this expression can be understood by considering the simple case of observing a single-frequency single-wavevector plane wave at $\omega_0 = n_0\omega_{\mathrm{rep}} + l\Omega$. Equation (1) can then be written in compact form by setting $A(x, y) = A_0$, $\phi(x, y) = k_x x + k_y y + \phi_0$, where A_0 and ϕ_0 are constants and k_x, k_y are the wavevector components that determine the propagation direction. Substituting Eq. (6) into Eq. (10), one obtains

$$F(k'_x, k'_y, n'\omega_{\mathrm{rep}}) = \begin{cases} \dfrac{A_0}{2} e^{i\phi_0} \delta(k_x - k'_x)\delta(k_y - k'_y)\delta_{n_0,n'} & (l = 1), \\ \dfrac{A_0}{2} e^{-i\phi_0} \delta(k_x + k'_x)\delta(k_y + k'_y)\delta_{n_0,-n'} & (l = -1). \end{cases} \tag{11}$$

The Fourier amplitude is finite at $(k'_x, k'_y, n'\omega_{\mathrm{rep}}) = (k_x, k_y, n_0\omega_{\mathrm{rep}})$ when $\omega_0 > n_0\omega_{\mathrm{rep}}$, whereas it is finite at $(k'_x, k'_y, n'\omega_{\mathrm{rep}}) = (-k_x, -k_y, -n_0\omega_{\mathrm{rep}})$ when $\omega_0 < n_0\omega_{\mathrm{rep}}$. Acoustic fields made up of a superposition of those with multiple n, l's and multiple wavevectors can be treated in a similar fashion.

To confirm the validity of our approach, we perform time-resolved imaging of electrically generated ~1 GHz surface acoustic waves on a GaAs substrate. Surface acoustic waves are produced in a RF-driven gold interdigital transducer deposited on the substrate surface. Surface displacements engendered by the acoustic waves are monitored by ultrashort probe light with interferometric detection.

Figure 1(a) shows a scanning electron micrograph of the sample surface. The gold electrodes making up the interdigital transducer (IDT) are fabricated by electron beam lithography and a liftoff technique on a semi-insulating Cr-doped GaAs (001) wafer. Five pairs of these electrodes are deposited with a spatial period of 3.4 μm and a thickness of 50 nm. The IDT orientation on the substrate is chosen to produce an applied electric field along the [110] direction, thus generating surface acoustic waves propagating in this direction.

Figure 1(b) shows a schematic diagram of the experimental setup. A function generator working at $f_0 = 834.10$ MHz is used to excite the IDT with an AC voltage amplitude 1.5 V at the electrodes. To probe the surface displacement caused by the propagating acoustic waves, we implement the probing apparatus of a standard optical pump–probe surface acoustic wave imaging setup.[17] The periodic probe light pulse train is generated by a mode-locked Ti–sapphire laser working at repetition frequency 75.677 MHz, central wavelength 830 nm, and pulse duration ~100 fs. The probe light beam, with average power 4 mW, is focused onto the sample surface with a ×50 microscope objective to detect the out-of-plane surface particle velocity at the optical probing point with an interferometer. (Strictly speaking, the interferometer output is proportional to the difference in the surface displacement

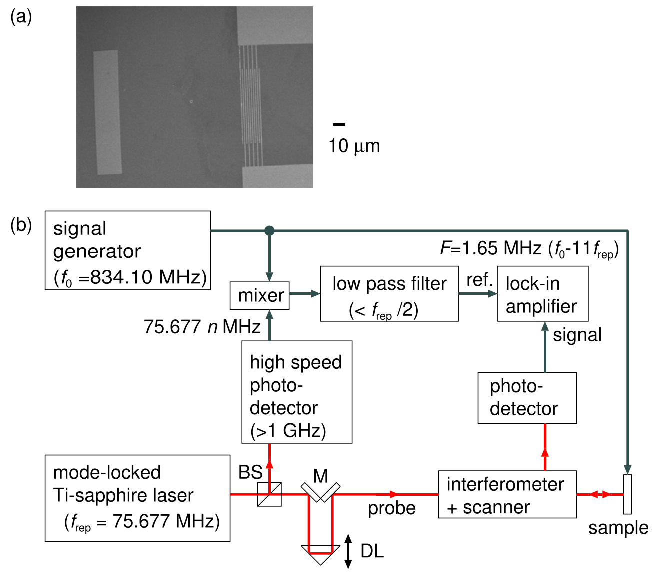

FIG. 1. (a) Scanning electron micrograph of the sample surface. The whiter region shows the gold electrodes. The interdigital transducer is visible on the right, whereas the rectangular gold-deposited area on the left serves to enhance the reflectivity of the sample. The spatial period of the transducer is 3.4 μm. (b) Schematic diagram of the experimental setup. BS: beam splitter, M: mirror, DL: optical delay line.

over a time interval of 300 ps.) The probe spot, of diameter ~1 μm, is scanned across a 120×120 μm^2 area to obtain a constant delay-time image of the acoustic field. A 0–4 m optical delay line is used for the probe light, corresponding to the range $\tau = 0$–13.21 ns (i.e., from 0 to T). The zero of τ has no physical meaning: only relative variations of quantities with respect to τ are of importance.

As detailed previously, the output of the interferometer photodetector is fed to a dual-phase lock-in amplifier, and the lock-in reference signal is obtained by use of a mixer [in our case a commercial double balanced mixer (DBM) module] that combines the output of a fast photodetector monitoring the laser pulses and the output of the function generator. The fast photodetector of bandwidth >1 GHz outputs multiple harmonics of the laser repetition frequency nf_{rep}. The output of the DBM contains frequency components $|f_0 \pm nf_{\mathrm{rep}}|$. Using a low pass filter (LPF) with a passband below $f_{\mathrm{rep}}/2$, we extract the required lowest frequency component involved in the DBM output for the lock-in amplifier reference. The reference signal frequency chosen is 1.65 MHz ($n_0 = 11$), which is automatically produced by the frequency mixing. The in-phase and quadrature outputs of the lock-in amplifier are recorded while scanning the probe spot position (x, y) and delay time τ, and are stored in the form $X(x, y, \tau)$ and $Y(x, y, \tau)$. The typical lock-in amplifier time constant is 30 ms for the probe spot scanning speed 10 μm/s. The overall spatial resolution, limited by the probe spot size, is ~1 μm.

Figure 2(a) shows a constant delay-time image of the in-phase signal $X(x, y, \tau = 0)$. By comparing Eqs. (1) and (4), one can understand that this represents a snapshot of the acoustic field $u(x, y, t)$ at a specific time t. The IDT electrodes are located outside the top right corner of the imaged area. (Photoconductive currents in the GaAs are avoided by this choice of scanning area.) Surface acoustic waves travel

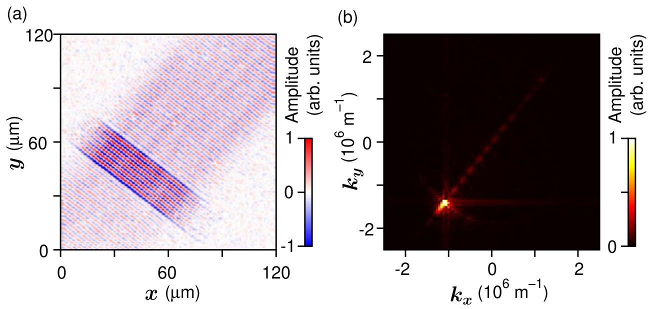

FIG. 2. (a) A constant delay-time image of $X(x, y, \tau)$ at $\tau = 0$ ps. The surface acoustic wave excitation is made outside of the upper right corner of the image. The waves propagate from the upper right corner toward the lower left corner. A stronger wave amplitude is observed on the gold-coated rectangular region situated at the lower left of the image center. (b) Fourier transform modulus $|F(k_x, k_y, \omega)|$ at $\omega = n_0\omega_{rep}$ with $n_0 = 11$ (with $n_0\omega_{rep} = 832.45$ MHz, corresponding to the acoustic wave frequency 834.10 MHz). A bright spot is observed at $(k_x, k_y) = (-1.11 \times 10^6, -1.45 \times 10^6)$ m^{-1}. Multimedia available online.

from the top right to the bottom left of the imaged area (Multimedia view: Movie 1). Visible in the scanned region is the rectangular region of deposited gold. Waves are more efficiently detected in this region because of the enhanced optical reflectivity there.

Figure 2(b) shows the experimental spatiotemporal Fourier transform modulus $|F(k_x, k_y, \omega)|$ at $\omega = n_0\omega_{rep}$ with $n_0 = 11$. This corresponds to the acoustic wave vibration frequency $75.677 \times 11 + 1.65 \simeq 834.10$ MHz. A bright spot is observed at $(k_x, k_y) = (-1.11 \times 10^6, -1.45 \times 10^6)$ m^{-1}. For this case of $\omega_0 > n_0\omega_{rep}$, the bright spot is observed at the actual wavevector of the propagating wave. For the case of $\omega_0 < n_0\omega_{rep}$, the bright spot would be observed at the inverted point, $(-k_x, -k_y)$ [see the discussion of Eq. (11)].

Figure 3(a) shows a cross section plot of the Fourier transform modulus of Fig. 2(b) along a line passing through the origin ($k_x = k_y = 0$) and the bright point, with the positive direction directed toward the top right. An intense peak is observed near -1.83×10^6 m^{-1}. The surface wave sound velocity is calculated to be 2.87×10^3 m/s, which is in good agreement with the literature value 2862.3 m/s for the [110] direction in GaAs (001).[26] Small oscillations with wave number arise because of the effect of the introduced rectangular gold-film region for a spatial Fourier transform evaluated over $120 \times 120\ \mu m^2$.

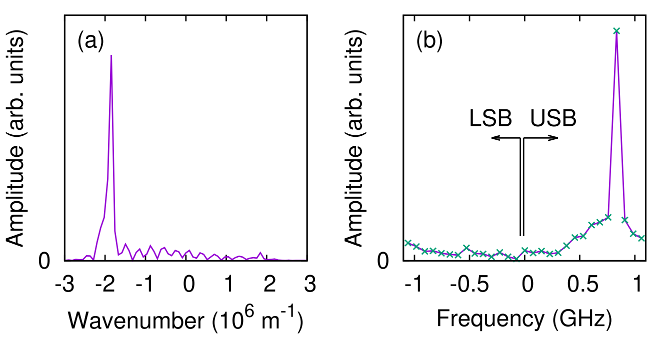

FIG. 3. (a) A cross section plot of the Fourier transform modulus shown in Fig. 2(b). The positive direction corresponds to the direction from bottom left to top right in Fig. 2(b). (b) The Fourier transform modulus at $(k_x, k_y) = (-1.11 \times 10^6, -1.45 \times 10^6)$ m^{-1} [corresponding to the brightest spot in Fig. 2(b)] as a function of frequency. The points with positive frequency correspond to the USBs, whereas those with negative frequency correspond to the LSBs. The lines connecting the points are a guide to the eye.

Figure 3(b) shows the frequency dependence of the Fourier transform modulus at $(k_x, k_y) = (-1.11 \times 10^6, -1.45 \times 10^6)$ m^{-1}, which corresponds to the location of the brightest spot in Fig. 2(b). The raw image data are subject to a detection sensitivity variation with respect to the delay time τ: this variation, about 30% over the whole time delay range, may be caused by an inaccurate alignment of the delay line. Such sensitivity variations give a spurious contribution to the Fourier spectrum. To understand this, consider multiplying the expression for u_N in Eq. (2) by a sensitivity variation function $f(\tau)$: the Fourier amplitude obtained from Eq. (11) for this modified u_N will then in general have non-zero spurious contributions around the main peak at $n' = n_0$ or $n' = -n_0$, which is the only peak expected for the ideal case in the absence of such contributions. To reduce such spurious contributions, before taking the temporal Fourier transform in Fig. 3(b), we compensate for the sensitivity variation to obtain an acoustic-field vibration amplitude that remains effectively constant on varying the delay time. The frequency in Fig. 3(b) corresponds to that of the acoustic waves, namely $nf_0 + F$. The positive frequencies ($n \geq 0$) correspond to USBs, whereas the negative frequencies ($n < 0$) correspond to LSBs (labeled by their absolute values). The amplitude, peaked at $f_0 = 834.1$ MHz, is greatly reduced at frequencies other than f_0, especially in the LSB region.

So far, we have considered a set of acoustic field images with different delay times. However, as we will see below, a delay time scan is not necessary for a linear system in which an acoustic vibration is expected only at the frequency f_0. For such a system, one can retrieve $A(x, y)$ and $\phi(x, y)$ in Eq. (1) from a single experimental image of $Z(x, y, \tau)$ at a fixed τ. For example, if $Z(x, y, \tau)$ is known at $\tau = 0$, one can then assume $Z(x, y, \tau) = Z(x, y, 0)\exp(-i\, l n_0\omega_{rep}\tau)$ with $l = \mathrm{sgn}(\omega_0 - n_0\omega_{rep})$. Equations (8) or (10) and (11) can then be used to obtain $A(x, y)$, $\phi(x, y)$ or $F(k_x, k_y, n_0\omega_{rep})$. In this case, one can avoid the problem of any unwanted variations of the overall detection sensitivity with τ. An animation of the acoustic field can be made with Eq. (1) by varying t (Multimedia view: Movie 2). By this means, not only does one avoid the need for precise delay line alignment and a longer data collection process at various τ, but one can construct animations at any desired temporal resolution without extra effort.

We have considered in our analysis a sample excited at a single frequency. If one excites with two or more different frequencies or makes use of broadband pulse excitation, it is possible to obtain independent measurements at each frequency by appropriate choice of the lock-in reference frequency.

In conclusion, we present an ultrafast time-resolved acoustic wave imaging technique in which arbitrary-frequency acoustic waves are excited asynchronously to the optical probe pulse train used to detect them. We demonstrate the method using single-frequency surface acoustic waves excited electrically with an interdigital transducer on GaAs at ~1 GHz. By exploiting a dual-phase lock-in amplifier with a reference signal synthesized from the gigahertz excitation signal and the laser pulse repetition rate, traveling acoustic waves can be imaged in two dimensions and also analyzed in k-space. This technique should be useful for studying electro-acoustic devices such as piezoelectric filters and sensors not only for surface acoustic waves but also for bulk waves. In general, the technique is applicable to any "pump"-probe measurement in which the pump and probe have different, fixed frequencies, including the case of broadband acoustic fields.

See the supplementary material for additional explanation for Multimedia views (the animation of surface acoustic wave images).

This work is partially supported by Grants-in-Aid for Scientific Research from the Japan Society for the Promotion of Science (21H05020). O.M. is partially supported by a research grant from Insight K.K.

AUTHOR DECLARATIONS

Conflict of Interest

The authors have no conflicts to disclose.

Author Contributions

Osamu Matsuda: Conceptualization (lead); Data curation (equal); Formal analysis (equal); Methodology (equal); Software (equal); Validation (equal); Writing – original draft (lead); Writing – review & editing (equal). **Shohei Ueno:** Conceptualization (supporting); Data curation (equal); Formal analysis (equal); Methodology (equal); Validation (equal). **Motonobu Tomoda:** Conceptualization (supporting); Methodology (equal); Software (equal). **Paul H. Otsuka:** Conceptualization (supporting); Data curation (equal); Formal analysis (equal); Methodology (equal); Validation (equal). **Oliver B. Wright:** Conceptualization (supporting); Formal analysis (equal); Writing – original draft (supporting); Writing – review & editing (equal).

DATA AVAILABILITY

The data that support the findings of this study are available from the corresponding author upon reasonable request.

REFERENCES

[1] C. C. W. Ruppel, "Acoustic wave filter technology—A review," IEEE Trans. Ultrason. Ferroelectr. Freq. Control **64**, 1390–1400 (2017).
[2] A. Kumar and R. Prajesh, "The potential of acoustic wave devices for gas sensing applications," Sens. Actuators, A **339**, 113498 (2022).
[3] C. Campbell, *Surface Acoustic Wave Devices and Their Signal Processing Applications* (Academic Press, San Diego, CA, 1989).
[4] J. W. Dally, "An introduction to dynamic photoelasticity," Exp. Mech. **20**, 409–416 (1980).
[5] R. E. Vines, M. R. Hauser, and J. P. Wolfe, "Imaging of surface acoustic waves," Z. Phys. B: Condens. Matter **98**, 255–271 (1995).
[6] J. V. Knuuttila, P. T. Tikka, and M. M. Salomaa, "Scanning Michelson interferometer for imaging surface acoustic wave fields," Opt. Lett. **25**, 613–615 (2000).
[7] M. Clark, S. D. Sharples, and M. G. Somekh, "Diffractive acoustic elements for laser ultrasonics," J. Acoust. Soc. Am. **107**, 3179–3185 (2000).
[8] Y. Sugawara, O. B. Wright, O. Matsuda, M. Takigahira, Y. Tanaka, S. Tamura, and V. E. Gusev, "Watching ripples on crystals," Phys. Rev. Lett. **88**, 185504 (2002).
[9] A. A. Maznev, A. M. Lomonosov, P. Hess, and A. A. Kolomenskii, "Anisotropic effects in surface acoustic wave propagation from a point source in a crystal," Eur. Phys. J. B **35**, 429–439 (2003).
[10] D. Shilo and E. Zolotoyabko, "Stroboscopic X-ray imaging of vibrating dislocations excited by 0.58 GHz phonons," Phys. Rev. Lett. **91**, 115506 (2003).
[11] C. Glorieux, K. Van de Rostyne, J. D. Beers, W. Gao, S. Petillion, N. V. Riet, K. A. Nelson, J. F. Allard, V. E. Gusev, W. Lauriks, and J. Thoen, "Acoustic waves at interfaces studied by laser ultrasonics," Rev. Sci. Instrum. **74**, 465–469 (2003).
[12] S. D. Sharples, M. Clark, and M. Somekh, "Surface acoustic wavefront sensor using custom optics," Ultrasonics **42**, 647–651 (2004).
[13] N. Wu, K. Hashimoto, K. Kashiwa, T. Omori, and M. Yamaguchi, "Study on the frequency dependence of lateral energy leakage in RF bulk acoustic wave device by fast-scanning laser probe system," Jpn. J. Appl. Phys., Part 1 **48**, 07GG01 (2009).
[14] A. Abbas, Y. Guillet, J. M. Rampnoux, P. Rigail, E. Mottay, B. Audoin, and S. Dilhaire, "Picosecond time resolved opto-acoustic imaging with 48 MHz frequency resolution," Opt. Express **22**, 7831–7842 (2014).
[15] A. Shaw, D. Teyssieux, and V. Laude, "A differential optical interferometer for measuring short pulses of surface acoustic waves," Ultrasonics **80**, 72–77 (2017).
[16] L. Zheng, L. Shao, M. Loncar, and K. Lai, "Imaging acoustic waves by microwave microscopy," IEEE Microwave Mag. **21**, 60–71 (2020).
[17] T. Tachizaki, T. Muroya, O. Matsuda, Y. Sugawara, D. H. Hurley, and O. B. Wright, "Scanning ultrafast Sagnac interferometry for imaging two-dimensional surface wave propagation," Rev. Sci. Instrum. **77**, 043713 (2006).
[18] D. M. Profunser, O. B. Wright, and O. Matsuda, "Imaging ripples on phononic crystals reveals acoustic band structure and Bloch harmonics," Phys. Rev. Lett. **97**, 055502 (2006).
[19] D. M. Profunser, E. Muramoto, O. Matsuda, O. B. Wright, and U. Lang, "Dynamic visualization of surface acoustic waves on a two-dimensional phononic crystal," Phys. Rev. B **80**, 014301 (2009).
[20] P. H. Otsuka, R. Chinbe, M. Tomoda, O. Matsuda, I. A. Veres, J.-H. Lee, J.-B. Yoon, and O. B. Wright, "Effect of excitation point on surface phonon fields in phononic crystals in real- and k-space," J. Appl. Phys. **117**, 245308 (2015).
[21] P. H. Otsuka, S. Mezil, O. Matsuda, M. Tomoda, A. A. Maznev, T. Gan, N. Fang, N. Boechler, V. E. Gusev, and O. B. Wright, "Time-domain imaging of gigahertz surface waves on an acoustic metamaterial," New J. Phys. **20**, 013026 (2018).
[22] P. H. Otsuka, R. Chinbe, M. Tomoda, O. Matsuda, Y. Tanaka, D. M. Profunser, S. Kim, H. Jeon, I. A. Veres, A. A. Maznev, and O. B. Wright, "Imaging phonon eigenstates and elucidating the energy storage characteristics of a honeycomb-lattice phononic crystal cavity," Photoacoustics **31**, 100481 (2023).
[23] T. Fujikura, O. Matsuda, D. M. Profunser, O. B. Wright, J. Masson, and S. Ballandras, "Real-time imaging of acoustic waves on a bulk acoustic resonator," Appl. Phys. Lett. **93**, 261101 (2008).
[24] S. Kaneko, M. Tomoda, and O. Matsuda, "A method for the frequency control in time-resolved two-dimensional gigahertz surface acoustic wave imaging," AIP Adv. **4**, 017124 (2014).
[25] O. Matsuda, S. Kaneko, O. B. Wright, and M. Tomoda, "Time-resolved gigahertz acoustic wave imaging at arbitrary frequencies," IEEE Trans. Ultrason., Ferroelectr., Freq. Control **62**, 584–595 (2015).
[26] M. M. de Lima, Jr., F. Alsina, W. Seidel, and P. V. Santos, "Focusing of surface-acoustic-wave fields on (100) GaAs surfaces," J. Appl. Phys. **94**, 7848–7855 (2003).